

Monte Carlo Simulation of Secondary Fluorescence in Small Particles and at Phase Boundaries

Xavier Llovet^{1,*}, Eero Valovirta², and Erkki Heikinheimo²

¹ Serveis Científic-Tècnics, Universitat de Barcelona, Lluís Solé i Sabarís, 1-3. 08028 Barcelona, Spain

² Helsinki University of Technology, Laboratory of Metallurgy, P. O. Box 6200, FIN-02015 Espoo, Finland

Abstract. Results from Monte Carlo simulations and experimental measurements of X-ray spectra of small Cu-particles in Fe-containing slags are presented. The analyzed Cu-particles remain suspended in flash smelting and Cu converter slags, which contain Fe up to about 33 wt%, and have diameters ranging from 5 up to 100 μm . Conventional standardless analysis of measured X-ray spectra gives an apparent Fe content of $\sim 1\text{--}5$ wt%, depending on the particle diameter, which cannot be explained in terms of the thermodynamic solubility of Fe in solid Cu. In order to study the influence of the Fe-containing slag to the apparent Fe content in the particles, X-ray spectra have been computed by means of Monte Carlo simulation of the coupled electron and photon transport. The simulation code used is largely based on the general-purpose simulation package PENELOPE and it incorporates ionization cross sections evaluated from an optical-data model and bremsstrahlung cross sections that reproduce radiative stopping power derived from partial wave calculations. Simulated Fe k -ratios, for different experimental situations, have been found to be in satisfactory agreement with measurements. The apparent Fe content is explained in terms of secondary fluorescence of Fe $K\alpha$ by Cu $K\alpha$ X-rays.

Key words: Secondary fluorescence; EPMA; particles.

In electron probe microanalysis (EPMA), the term secondary fluorescence usually refers to the emission

of characteristic (fluorescent) X-rays generated by photoelectric absorption of X-rays produced by electron impact. For homogeneous samples, a number of approximate analytical corrections have been proposed to account for this effect (see e.g. [1] and references therein). However, the range of X-ray penetration (absorption) and thus the range of generation of secondary fluorescence can be one to two orders of magnitude greater than the range of electron penetration [2]. Consequently, a particular sample assumed to be homogeneous as regards electron penetration, can be non-homogeneous as regards secondary fluorescence production. This situation is found when we analyze relatively small particles embedded in a matrix and/or when we analyze near to the boundary between two different media. The contribution of secondary fluorescence is usually small and it is commonly approximated by very crude methods or even neglected. However, in some situations, this contribution can be important and must be taken into consideration carefully. For example, when analyzing trace contents of an element in a phase that is close to another phase containing a high concentration of an element capable of exciting the element of interest. In this case, even if we analyse relatively far from the phase boundary, the effect of secondary fluorescence may largely affect the results not only quantitatively but also qualitatively (see e.g. [3, 4]).

The contribution of secondary fluorescence can be minimised by using L -lines instead of K -lines in the quantitative procedure [5]. However, measurement and quantification using L -lines is difficult and

* To whom correspondence should be addressed

affected by larger uncertainties. Secondary fluorescence corrections have been proposed for non-homogeneous targets, such as multilayers (see e.g. [6] and references therein), near phase boundaries [3] and for spherical particles [3, 7]. Those corrections usually require numerical integration. For example, Armstrong and Buseck [7] calculated secondary fluorescence in spherical particles and selected materials by means of a six-fold numerical integration. On the other hand, these corrections depend on the particular geometry and changing to another geometry may be quite tedious. Alternatively, Monte Carlo simulation of electron transport has been used to predict the secondary radiation induced at phase boundaries [8]. In all these cases, a separate correction is required to account for the fluorescence induced by characteristic X-rays and by bremsstrahlung. A powerful approach to computing secondary fluorescence consists in using Monte Carlo simulation to calculate the coupled transport of electrons and photons in the target, as pointed out recently by Acosta et al. [9]. Indeed, by simulating the coupled electron-photon transport, the calculation of secondary fluorescence includes both the contribution of characteristic and bremsstrahlung X-rays, and, it can be easily generalized to complex geometries. In fact, this generalization simply consists in defining the appropriate geometry in the simulation code, which can be straightforwardly done by using available dedicated geometry packages [10].

In this work, we address the problem of analysing small Cu-particles suspended in flash smelting and Cu converter slags, which contain Fe up to about 33 wt% [11]. By using conventional quantitative EPMA procedure, the apparent Fe content of the particles (using the $K\alpha$ line) was found to depend strongly on the particle diameter: the smaller the particle, the higher the Fe concentration. Thus, for particles with apparent diameters greater than $\sim 50 \mu\text{m}$, the amount of Fe found was $\sim 1 \text{ wt}\%$, while for particles with diameters less than $\sim 10 \mu\text{m}$ the Fe content was in the range 3–5 wt%. In process conditions the slag is cooled very slowly, taking about one day to cool down. Hence, supersaturation should not be possible and thus thermodynamic equilibrium between the metal and the slag can be assumed. The thermodynamic solubility of Fe in solid Cu was calculated from the SGTE [12] data for the simple binary Cu-Fe system: at 298 K it is negligible at $5.3 \times 10^{-9} \text{ wt}\%$. The particle metal contains some impurities (Sn, Sb,

As and S) that are highly unlikely to decrease the activity of iron in copper so much (9 orders of magnitude) that the observed Fe content would be possible. Therefore, the observed Fe content must be mainly caused by secondary fluorescence of Fe by $\text{Cu } K\alpha$ radiation.

In order to calculate the contribution of secondary fluorescence to the emitted Fe X-rays, we have simulated emission X-ray spectra using the Monte Carlo simulation algorithm developed by Acosta et al. [9]. This algorithm is largely based on the general-purpose simulation package PENELOPE [13] and incorporates ionization cross sections evaluated from an optical-data model and bremsstrahlung cross sections that reproduces radiative stopping powers derived from partial wave calculations. The aim of this work is to show, with an example of practical interest, that secondary fluorescence effects in complex geometries can be easily quantified by using Monte Carlo simulation of coupled photon-electron transport.

Experimental

In order to study the effect of secondary fluorescence in the Cu-particles, two samples were selected. The samples were mounted in epoxy, sectioned and polished following conventional metallo-

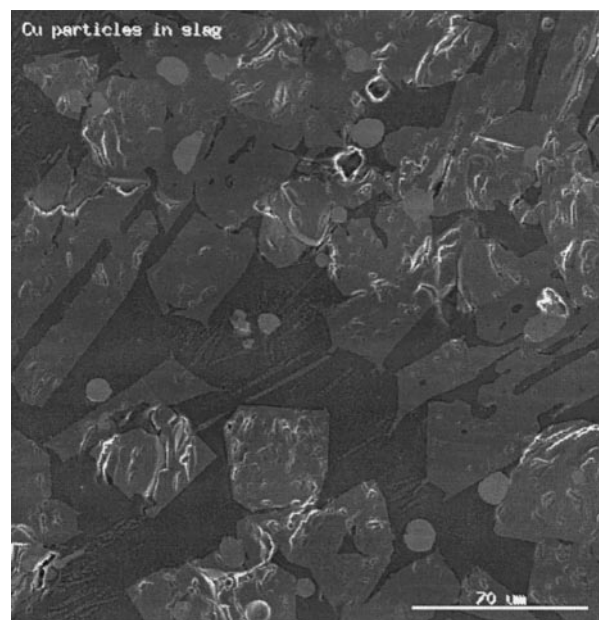


Fig. 1. Backscattered electron micrograph of a polished section of the analysed Cu-particles in the Fe-containing slag. Cu-particles are the bright circles, with diameters between 10 and 20 μm . The slag consists of two phases, a polygonal (grey) phase and a dark phase

graphics procedures. Polishing was finished with 1- μm diamond paste. The average bulk composition of the slags in each sample was obtained by X-ray fluorescence analysis and it was the following (in wt%): Pb 0.25, Zn 2.16, Cu 1.69, Ni 0.04, Fe 41.9, S 0.17, Si 14.58, O 39.2, for the first sample, and Pb 0.26, Zn 2.20, Cu 1.47, Ni 0.03, Fe 40.7, Co 0.05, S 0.13, Si 15.23, O 39.3, for the second sample. Oxygen was calculated by difference to 100%. Figure 1 shows a backscattered electron micrograph of a polished section of the analyzed sample. In this case, the slag is mainly composed by two phases. The composition given above is the average of the two phases.

X-ray spectra were acquired in a large number of Cu-particles, at different positions from the center of the particle to the boundary. Measurements were performed at accelerating voltages of 15 and 25 keV on a JEOL JXA-840 scanning electron microscope with a Noran Voyager energy-dispersive spectrometer, having a take-off-angle of 40°. The detector is a Si(Li), with a ultra-thin window. In the acquisitions, the solid angle subtended by the detector was 0.0012 sr. Beam currents were about $\sim 1\text{--}2$ nA, selected to minimize dead time. Acquisition (live) times were 100 s. Particle shapes and (apparent) diameters, i.e. the diameter measured in the cross section of the sample, were determined optically by inspection of the electron micrographs, and were found to be in the range 5–60 μm . Spectra were mainly acquired in spherical particles, which had apparent diameters in the range from 9 to 20 μm . In each spectrum, the Fe K -ratio was determined by dividing the net X-ray intensity of the Fe $K\alpha$ peak to the X-ray intensity obtained from an X-ray spectrum of a pure, bulk, Fe standard.

Monte Carlo Simulation

The Monte Carlo simulation code used in this work has been developed by Acosta et al. [9]. The code performs Monte Carlo simulation of electron-photon showers by using a modified version of the PENELOPE [13] code system and provides the X-ray spectra at a given direction. PENELOPE is a general-purpose simulation package which generates electron-photon showers in homogeneous media, of arbitrary composition, for a wide energy range, from about 1 keV up to about 1 GeV. PENELOPE also includes a geometry package for simulation of complex geometries consisting of homogeneous bodies limited by quadric surfaces. The complete code system (FORTRAN source files and data base) is available from the NEA data bank [14]. The cross sections implemented in the code as well as the simulation algorithm (i.e. the set of rules to generate random electron trajectories from a given scattering model) have been described in detail elsewhere [15, 9]. Here, we summarize the major features of the simulation algorithm.

Electron Transport

Elastic scattering of electrons is simulated using a combination of the Wentzel (screened Rutherford)

differential cross section (DCS) and a fixed-angle scattering process. This analytical DCS contains three parameters that are determined in such a way that the mean free path between collisions and the mean and the variance of the angular deflection in each elastic collision are identical with the values obtained with a realistic numerical DCS. The model is thus completely determined by the values of the mean free path and the first and second transport mean free paths, which have been calculated for all elements using a partial-wave method with the Dirac-Hartree-Fock-Slater field, corrected for exchange effects.

Inelastic collisions are described in terms of analytical DCSs based on a simple generalized oscillator strength (GOS) model proposed by Liljequist [16]. In this model the ionization of each atomic electron shell is described by a single oscillator, whose “resonance energy” is calculated in such a way that the mean excitation energy I tabulated by Berger and Seltzer [17] is exactly reproduced. This model yields stopping powers that coincide with the values recommended by Berger and Seltzer for energies above 10 keV, and is expected to remain accurate for much smaller energies, down to a few hundred eV.

PENELOPE generates electron trajectories as a series of “free flights” between consecutive interactions. Along each free flight, the energy E of the electron is assumed to stay constant. To simulate the generation of characteristic X-rays, which result from vacancies produced in a K -shell, in each free flight we calculate the probability that an ionization is produced, using the total ionization cross section computed from the optical-data model of Mayol and Salvat [18]. This cross section has been recently shown to give reliable results for K -shell ionization [19]. After computing the ionization probability, we sample a random number uniformly in $(0, 1)$ and consider that the interaction is effective only when the random number is less than the ionization probability. When an ionization occurs, its position is sampled uniformly along the free flight. As the probability of ionization in a free flight is much less than unity, this procedure gives the correct average number of ionizations per unit path length. Excited ions relax to their ground state by migration of the initial vacancy to outer electron shells, which proceeds through emission of fluorescent X-rays or Auger electrons with characteristic energies. Our code, as well as PENELOPE, simulates the emission of

characteristic X-rays that result from vacancies produced in a K -shell. We consider only characteristic photons emitted in the first stage of the de-excitation cascade, i.e. when the initial vacancy in the K -shell is filled by an electron from an outer shell. The probability that a radiative de-excitation occurs is obtained from the fluorescence yields tabulated by Fink and Rao [20]. The considered characteristic photons are $K\alpha$ and $K\beta$, with relative probabilities obtained from the line fractions given by Khan and Karimi [21]. Characteristic X-rays are assumed to be emitted isotropically.

Bremsstrahlung emission is described by means of a double differential cross section (DDCS) which is a combination of the modified Bethe-Heitler DCS [22, 23], with the angular distribution derived from the Kirkpatrick-Wiedmann-Statham DCS [24, 25]. The DDCS is normalized in such a way that it exactly reproduces the radiative stopping powers computed from partial-wave calculations [26]. This DCS provides a fairly good approximation for the electron mean free path between radiative events and for the distribution of energy losses in those events, as well as for the angular distribution of emitted photons [9].

Although the simulation of electron tracks may be performed on the basis of a mixed procedure, in our simulations we have used the detailed method (interaction by interaction). Interface crossings between two media with different compositions are handled as follows: when the particle arrives at a surface separating both media it is stopped after the interface, and simulation is continued using the scattering data for the new medium. To improve the efficiency of the simulation, we apply interaction forcing to both characteristic and bremsstrahlung emission processes (see e.g. [27]).

Photon Transport

The considered photon interactions are coherent (Rayleigh) scattering, incoherent (Compton) scattering and photoelectric absorption. The cross sections implemented in PENELOPE are given by simple analytical formulae, with parameters determined from fits to updated interaction data from different sources, mainly Cullen et al. [28] and Berger and Hubbell [29]. All random variables are generated by using purely analytical expressions, so that the structure of the simulation code is very simple.

The DCS for coherent scattering is the Rayleigh formula, with the atomic form factor given by a simple rational expression with parameters determined from a fit to the numerical form factors tabulated by Hubbell et al. [30]. Compton scattering is simulated by means of the relativistic impulse approximation [31], which accounts for Doppler broadening and binding effects. Photoelectric cross sections are obtained by interpolation in a table generated with the XCOM program of Berger and Hubbell [29].

Results and Discussion

The Monte Carlo simulation code, as described above, generates energy distributions of X-rays emitted from the specimen, per incident electron and per unit solid angle, in the direction of the X-ray detector. To calculate each theoretical spectrum we have simulated 200,000 primary electron tracks. The statistical uncertainties of the results in the characteristic peaks are then less than 5%.

The diameter d_a of the circular section that results from the (random) plane polishing of a spherical particle is evidently different from the real diameter of the 3D particle. In order to take this fact into account, we have simulated X-ray spectra for inclusions with different diameters d_i , which produce circular sections with the same diameter when sectioned by the polishing procedure. Namely, we have simulated inclusions for three different ratios P/d_i , where P is the thickness of the inclusion and d_i is the diameter

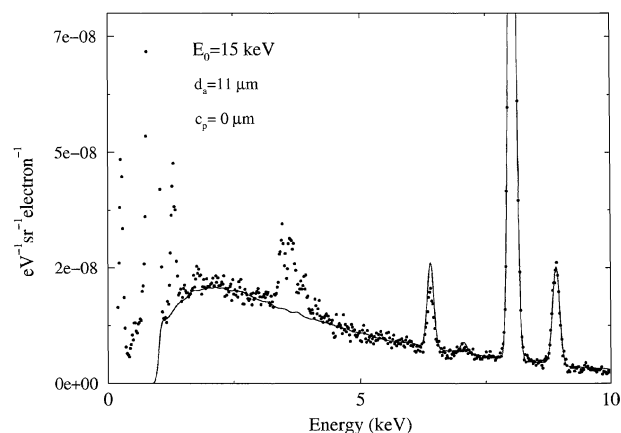


Fig. 2. Simulated (solid line) and experimental (dots) X-ray spectrum from a 11- μ m-diameter Cu-particle, generated by 15 kV electron beam at normal incidence. The spectrum was acquired at the center of the particle

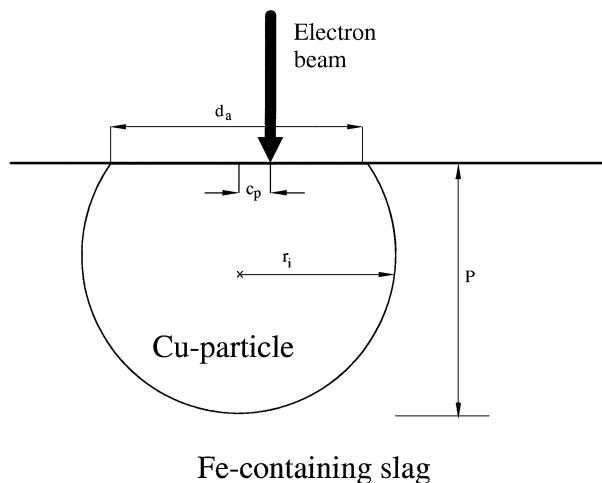


Fig. 3. Geometry of the spherical Cu-inclusion embedded in a Fe-containing matrix. P is the inclusion thickness (maximum depth), d_a is the apparent diameter observed in the polished section, r_i is the radius of the inclusion and c_p is the distance of the impact point of the electron beam to the center of the inclusion

(see Fig. 2). This scheme is similar to the one adopted by Gauvin et al. [32]. In particular, simulations have been performed for $P=0.5 d_i$, which represents a particle that has been sectioned by a plane through its origin, and for two extremes cases, namely, when $P=0.5 d_i$, and when $P=0.5 d_i$. The latter cases represent two inclusions sectioned in such a way that, after polishing, only a small volume of the particle remains beneath the surface (the first one) and almost the entire inclusion is in the polished sample (the second one). Figure 3 shows the geometry of a spherical inclusion embedded in a matrix, as used for simulation purposes.

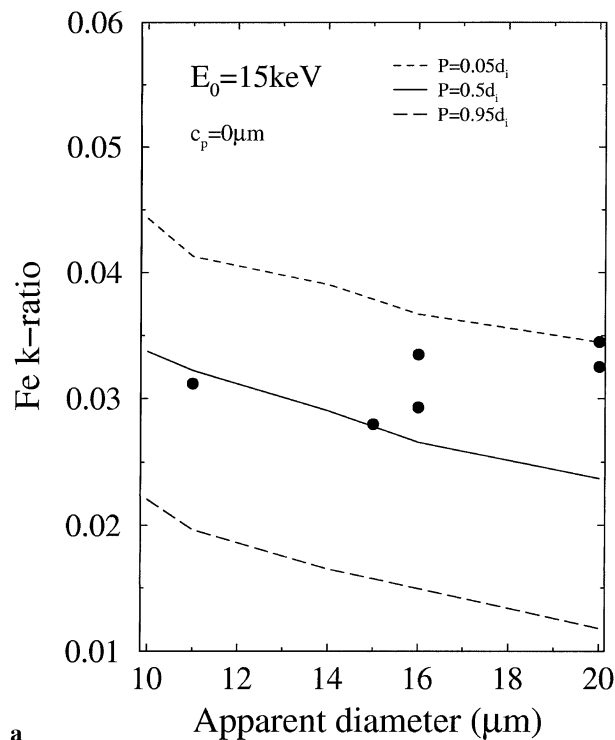
X-ray spectra have been simulated for a number of different spherical particles, for different positions of the incident electron beam and for the three ratios P/d_i , as explained above. Simulations have been performed at accelerating voltages of 15 and 25 keV, for the two different slag compositions. Figure 2 shows the comparison of a simulated and experimental spectrum, for 15 keV electrons incident energy, of a 11- μm -diameter Cu-particle, taken at the center of the particle. In this case, the simulated spectrum has been convoluted with a Gaussian response function with energy dependent full width at half maximum, determined experimentally. To compare with simulation, the experimental spectrum has been converted to absolute units by using the equation $N(E) = N_{\text{ch}} / (N_0 \varepsilon \Delta \Omega \Delta E)$ where N_{ch} is the number of counts in a particular photon channel, N_0 is the total

number of incident electrons, $\Delta \Omega$ is the solid angle subtended by the detector and ε is the detection efficiency. Unfortunately, the actual version of the code does not allow to transport photons with energies lower than 1 keV. For comparison purposes, we have assumed that the efficiency is unity, which is plausible for energies greater than 1 keV for windowless detectors. On the other hand, the actual version of the code does not allow the simulation of characteristic photons resulting from L - and M -shell ionization. Therefore, the L -lines that appear in the low-energy region of the experimental spectra could not be reproduced. These peaks correspond to elements present in the particle, namely Cu and impurities such as Sn, Sb, As and S.

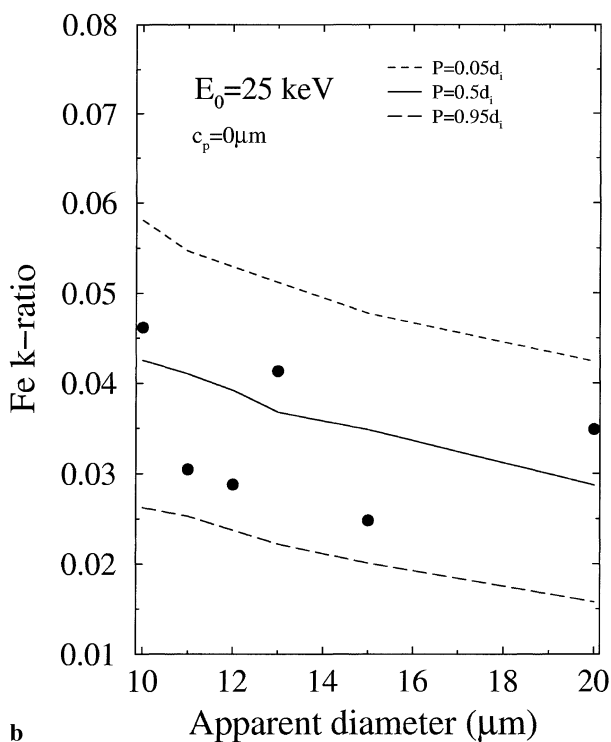
When comparing simulations with experimental data, the following should be noted. First, we have selected only circular sections that would correspond to spherical particles. However, even if the section is perfectly circular, the particle can obviously be of irregular shape beneath the section. On the other hand, the slag is mainly composed by two phases and we have used the mean composition of the two phases. Therefore, the possible local variation of the slag composition has not been taken into account.

Figure 4 shows the comparison of simulated and experimental Fe k -ratios, considered as functions of the apparent diameter of the inclusion, for incident electron energies of 15 and 25 keV. Simulations are displayed for the indicated values of the ratio P/d_i , as defined previously. In all the cases, experimental spectra were taken at the center of the inclusion. The contribution of secondary fluorescence is seen to decrease for increasing particle sizes, until X-rays are completely absorbed within the particle and secondary (K - K) fluorescence ceases to be possible. We can see that experimental values lie within the “error” band that corresponds to the extreme values of the ratio P/d_i , and therefore the agreement can be considered satisfactory. In order to explore the range of secondary fluorescence in a more general case, simulations have been performed for pure spherical Cu-inclusions (with $P/d_i=0.83$) embedded in a pure Fe-matrix, at 15 keV electron incident energies (Fig. 5). We can see that even for inclusions of ~ 50 - μm -diameter, the emission of Fe X-rays due to secondary fluorescence is not negligible and may give raise to an unrealistic Fe concentration in the particles.

Figure 6 shows the comparison of simulated and experimental Fe k -ratios, as a function of the distance



a



b

Fig. 4. Simulated (line) and experimental (dots) Fe k -ratios as a function of the apparent inclusion diameter for 15 keV (a) and 25 keV (b) electron incident energies. Dashed, solid and long-dashed lines correspond to simulated inclusions with $P = 0.05 d_i$, $P = 0.5 d_i$ and $P = 0.95 d_i$, respectively (for explanation, see the text). The electron beam impacts at the center of the inclusions

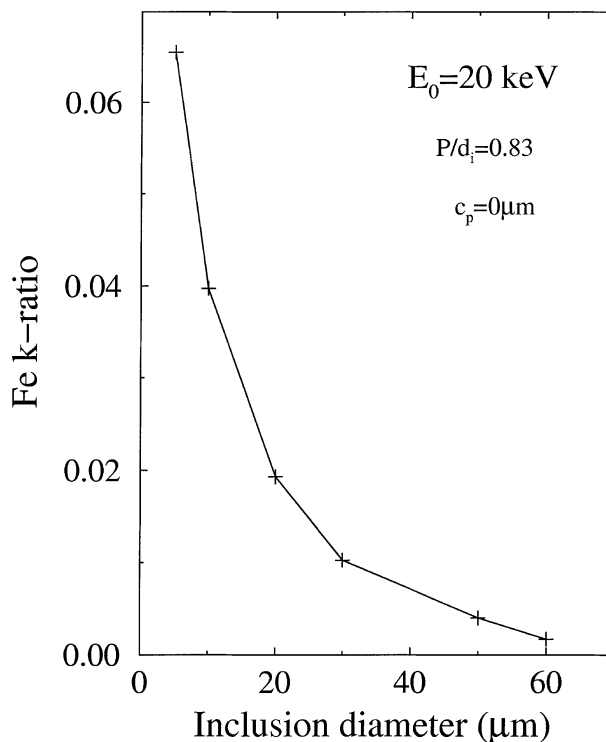


Fig. 5. Simulated Fe k -ratios emitted from spherical pure Cu-particles embedded in a pure Fe-matrix, as a function of the inclusion diameter, for 15 keV electron incident energies. The electron beam impacts at the center of the inclusions

of the point of electron impact to the center of the inclusion, for Cu-particles of different apparent diameters and for incident electron energies of 15 and 25 keV. We can see that the secondary fluorescence increases when spectra are taken at points of impact closer to the boundary. In almost all the analyzed cases, experimental data were found to agree with simulation satisfactorily, i.e. experimental points were found to lie within the “error” band of the real diameter estimation, as explained above. Obviously, when the spectrum is simulated or acquired very close to the boundary, the fluorescence of Fe is also the result of the direct ionization of electrons penetrating the surrounding matrix. Indeed, the effective ionization electron range (defined as the average path length that the electrons travel before slowing down to an energy equal to the ionization energy of the shell) is $\sim 3.2 \mu\text{m}$ at 25 keV and $\sim 1.3 \mu\text{m}$ at 15 keV. Therefore, spectra taken at a distance less than these values will contain Fe X-rays originated by direct impact of electrons penetrating the Fe-containing matrix. To show this effect, simulations have been performed disregarding ionization produced by direct electron

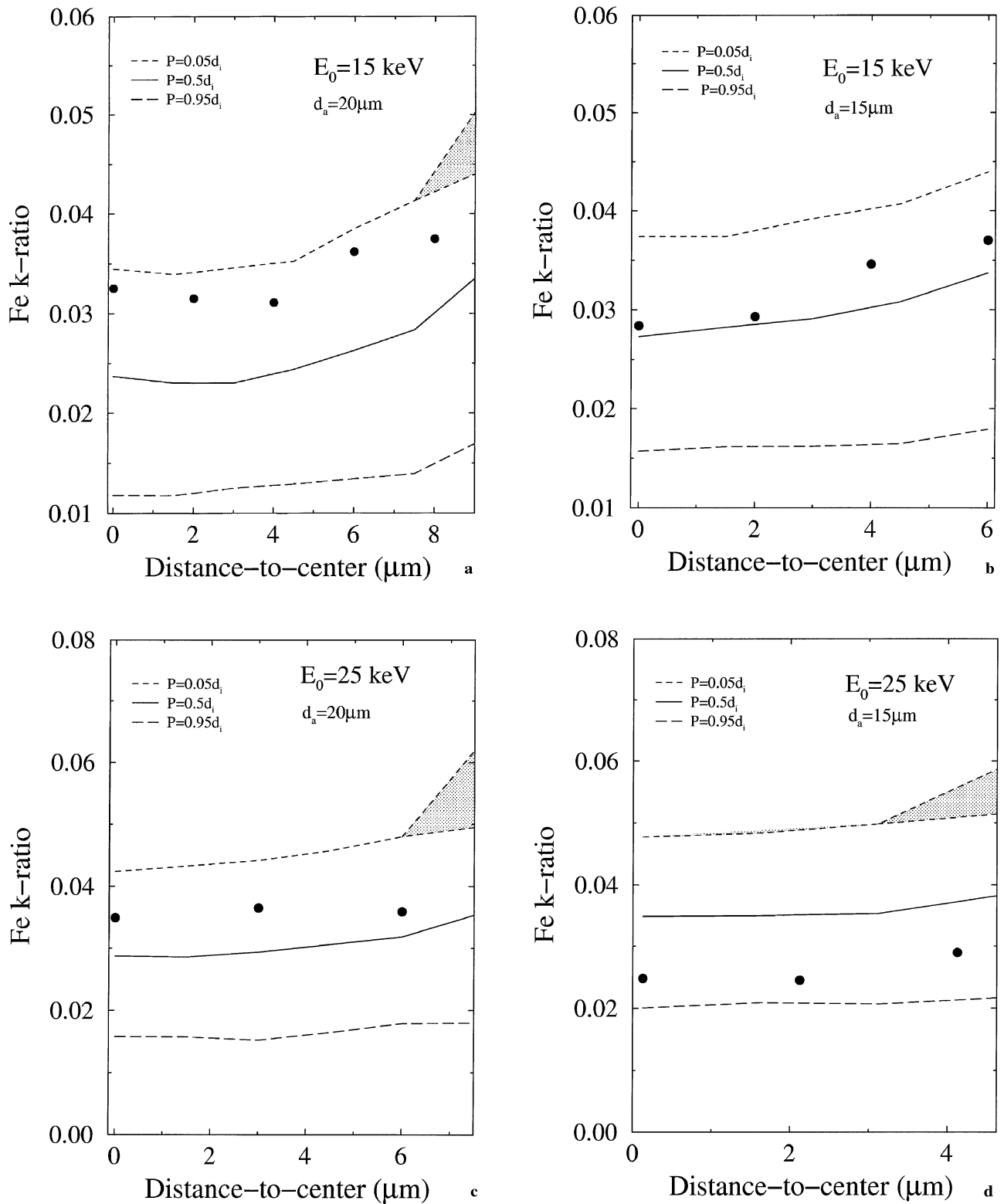


Fig. 6. Simulated (lines) and experimental (dots) Fe k -ratios as a function of the distance from the electron point of impact to the center of the inclusion, for different electron incident energies and particle diameters, as indicated in the figures. Dashed, solid and long-dashed lines correspond to simulated inclusions with $P=0.05 d_i$, $P=0.5 d_i$ and $P=0.95 d_i$, respectively (for explanation, see the text). Shadow areas represent the contribution to the fluorescence of direct electron impact ionization in the matrix

impact in the matrix. The shadow areas in Fig. 6 represent the contribution to the total fluorescence of electrons penetrating the Fe-containing matrix.

In conclusion, we have shown that Monte Carlo simulation of electron-photon showers gives reliable results as regards secondary fluorescence in Cu-particles embedded in Fe-containing slag. With the aid of available geometry packages, the simulation can be extended in straightforward manner to particles with other shapes and also to other kind of geometries.

Acknowledgements. The authors wish to thank Dr. F. Salvat for helpful discussions and for critically reading the manuscript.

References

- [1] S. J. B. Reed, *Electron Microprobe Analysis*. Cambridge University Press, Cambridge, 1993.
- [2] M. Green, *Proc. Phys. Soc.* **1964**, 83, 435.
- [3] G. F. Bastin, F. J. J. van Loo, P. J. C. Vosters, J. W. G. A. Vrolijk, *Scanning* **1983**, 5, 172.
- [4] P. Maaskand, H. Kaper, *Mineral. Mag.* **1991**, 55, 277.
- [5] C. Fournier, S. Lequeux, C. Fucili, F. Le Guyadec, C. Merlet, *Proc. 3rd Regional Workshop EMAS'98*. In: X. Llovet, C. Merlet, F. Salvat (Eds.) University of Barcelona, Barcelona, 1998, p. 343.
- [6] R. A. Waldo, *Microbeam Analysis*. In: D. G. Howitt (Ed.) San Francisco Press, San Francisco, 1991, p. 45.
- [7] J. T. Armstrong, P. R. Buseck, *X-Ray Spectrom.* **1985**, 14, 173.
- [8] D. E. Newbury, R. L. Myklebust, *Scanning Suppl.* **1994**, 16, IV, IV-2.
- [9] E. Acosta, X. Llovet, E. Coleoni, J. A. Riveros, F. Salvat, *J. Appl. Phys.* **1998**, 83, 6038.
- [10] F. Salvat, *Radiation Physics Group, Internal Report no. UBRPG-1998-01*. Barcelona, 1998.
- [11] E. Heikinheimo, H. Jalkanen, *Proc. 3rd Regional Workshop EMAS'98*. In: X. Llovet, C. Merlet, F. Salvat (Eds.) University of Barcelona, Barcelona, 1998, p. 345.
- [12] SGTE, *The Scientific Group Thermodata Europe*, see e.g. <http://www.thermocalc.se/>.
- [13] J. Baró, J. Sempau, J. M. Fernández-Varea, F. Salvat, *Nucl. Instrum. Meth. B* **1995**, 100, 31.
- [14] OECD Nuclear Energy Agency Data Bank, Le Seine Saint-Germain, 12 Boulevard des Iles, 92130 Issy-les-Moulineaux, France (e-mail: NEA@db.nea.fr).
- [15] J. Sempau, E. Acosta, J. Baró, J. M. Fernández-Varea, F. Salvat, *Nucl. Instrum. Meth. B* **1997**, 132, 377.
- [16] D. Liljequist, *J. Phys. D: Appl. Phys.* **1983**, 16, 1567.
- [17] M. J. Berger, S. M. Seltzer, *National Bureau of Standards, Report NBSIR 82-2550* Washington, 1982. Also available as ICRU Report 37, 1984.
- [18] R. Mayol, F. Salvat, *J. Phys. B: At. Mol. Opt. Phys.* **1990**, 23, 2117.
- [19] X. Llovet, C. Merlet, F. Salvat, *J. Phys. B: At. Mol. Opt. Phys.* submitted.
- [20] R. W. Fink, P. Venogulapa Rao, *Handbook of Spectroscopy*. In: J. W. Robinson (Ed.) Vol. 1. CRC Press. Cleveland, Ohio. 1974, p. 219.
- [21] Md. R. Khan, M. Karimi, *X-Ray Spectrom* **1980**, 9, 32.
- [22] H. Bethe, W. Heitler, *Proc. Roy. Soc. (London)* **1934**, A146, 83.
- [23] F. Salvat, J. M. Fernández-Varea, *Nucl. Instrum. and Meth. B* **1992**, 63, 255.
- [24] P. Kirkpatrick, L. Wiedmann, *Phys. Rev.* **1945**, 67, 321.
- [25] P. J. Statham, *X-ray Spectrom.* **1976**, 5, 154.
- [26] L. Kissel, C. A. Quarles, R. H. Pratt, *At. Data Nucl. Data Tables* **1983**, 28, 381.
- [27] A. F. Bielajew, D. W. O. Rogers, *Nucl. Instr. and Meth.* **1987**, B18, 165.
- [28] D. E. Cullen, M. H. Chen, J. H. Hubbell, S. T. Perkins, E. F. Plechaty, J. A. Rathkopf, J. H. Scofield, *Lawrence Livermore National Laboratory, Report UCRL-50400*, vol. 6, rev. 4, parts A and B, 1989.
- [29] M. J. Berger, J. H. Hubbell, *National Bureau of Standards, Report NBSIR 87-3797*, Washington, 1987.
- [30] J. H. Hubbell, W. J. Veigele, E. A. Briggs, R. T. Brown, D. T. Cromer, R. J. Howerton, *J. Phys. Chem. Ref. Data* **1975**, 4, 471. Erratum: *ibid.* **1977**, 6, 615.
- [31] D. Brusa, G. Stutz, J. A. Riveros, J. M. Fernández-Varea, F. Salvat, *Nucl. Instr. and Meth.* **1996**, A 379, 167.
- [32] R. Gauvin, G. L'Espérance, S. St-Laurent, *Scanning* **1992**, 14, 37.